Influence of image resolution and evaluation algorithm on estimates of the lacunarity of porous media

D. E. Pendleton,* A. Dathe,† and P. Baveye‡
Laboratory of Geoenvironmental Science and Engineering, Bradfield Hall, Cornell University, Ithaca, New York 14853, USA
(Received 8 February 2005; published 20 October 2005)

In recent years, experience has demonstrated that the classical fractal dimensions are not sufficient to describe uniquely the interstitial geometry of porous media. At least one additional index or dimension is necessary. Lacunarity, a measure of the degree to which a data set is translationally invariant, is a possible candidate. Unfortunately, several approaches exist to evaluate it on the basis of binary images of the object under study, and it is unclear to what extent the lacunarity estimates that these methods produce are dependent on the resolution of the images used. In the present work, the gliding-box algorithm of Allain and Cloitre [Phys. Rev. A **44**, 3552 (1991)] and two variants of the sandbox algorithm of Chappard *et al.* [J. Pathol. **195**, 515 (2001)], along with three additional algorithms, are used to evaluate the lacunarity of images of a textbook fractal, the Sierpinski carpet, of scanning electron micrographs of a thin section of a European soil, and of light transmission photographs of a Togolese soil. The results suggest that lacunarity estimates, as well as the ranking of the three tested systems according to their lacunarity, are affected strongly by the algorithm used, by the resolution of the images to which these algorithms are applied, and, at least for three of the algorithms (producing scale-dependent lacunarity estimates), by the scale at which the images are observed. Depending on the conditions under which the estimation of the lacunarity is carried out, lacunarity values range from 1.02 to 2.14 for the three systems tested, and all three of the systems used can be viewed alternatively as the most or the least "lacunar." Some of this indeterminacy and dependence on image resolution is alleviated in the averaged lacunarity estimates yielded by Chappard *et al.*'s algorithm. Further research will be needed to determine if these lacunarity estimates allow an improved, unique characterization of porous media.

DOI: 10.1103/PhysRevE.72.041306 PACS number(s): 81.05.Rm, 61.43.Hv, 95.75.Mn

I. INTRODUCTION

Over the last two decades, a significant body of research has been devoted to quantifying the fractal characteristics of natural or manufactured porous media. Motivation for this effort initially arose from the hope of encapsulating in a single number—the fractal dimension—the intricate geometry of the interstitial space, and of using this number to predict a range of other properties of porous media. As in other disciplines [1–3], this hope has since been severely dashed for a number of practical reasons, including the facts (1) that the physical nature of porous media requires consideration of not one but three distinct fractal dimensions, associated respectively with the pores, the solid phase, and the pore-solid interfaces [4,5], (2) that each of these dimensions can be evaluated with a variety of algorithms, often yielding different estimates [4,6], and (3) that, when the evaluation algorithm relies on pictures of the porous media, the resolution of these pictures and their prior treatment (e.g., segmentation or thresholding) can influence significantly the fractal dimension estimates that are obtained [5,7–12].

Aside from these practical difficulties, perhaps the most fundamental problem with the application of fractal geometry to porous media is that it is unclear why the hope of encapsulating the intricate geometry of porous media in a single index ever arose in the first place. Indeed, at the same time he coined the term "fractal", Mandelbrot [13] pointed out that fractal dimensions would not suffice to provide a satisfactory description of the geometry of lacunar fractals, and that at least one other parameter, which he termed "lacunarity," is necessary. The key reason for this requirement is vividly illustrated by the fact that Sierpinski carpets (Fig. 1) that have greatly different appearances, and therefore would likely behave differently if they were physical objects, can nevertheless have precisely the same fractal (similarity) dimension. Therefore, the fractal dimension alone is not a very reliable diagnostic of the geometry and properties of lacunar fractals, and any attempt to find a unique relationship between the fractal dimension and any particular feature (e.g., transport or dielectric properties) of a porous medium is most probably doomed to failure, unless it also accounts explicitly for the lacunarity of the porous medium.

Mandelbrot [13–15] introduced the concept of lacunarity as a measure of the distribution of gap sizes in a given geometric object. In other words, lacunarity can be thought of as a measure of the "gappiness" or "holiness" of a geometric structure [6]. Objects are more lacunar if their gap sizes are distributed over a wider range. In that sense, the Sierpinski carpet of Fig. 1(a) is more lacunar than that of Fig. 1(c). A more precise definition of lacunarity was introduced by Gefen *et al.* [16], who viewed lacunarity as a measure of the

*Present address: Dept. of Earth and Atmospheric Sciences, Bradfield Hall, Cornell University, Ithaca, NY 14853, USA.
†Present address: Dept. of Biological and Environmental Engineering, Riley-Robb Hall, Cornell University, Ithaca, NY 14583, USA.
‡Corresponding author. Electronic address: Philippe.Baveye@cornell.edu

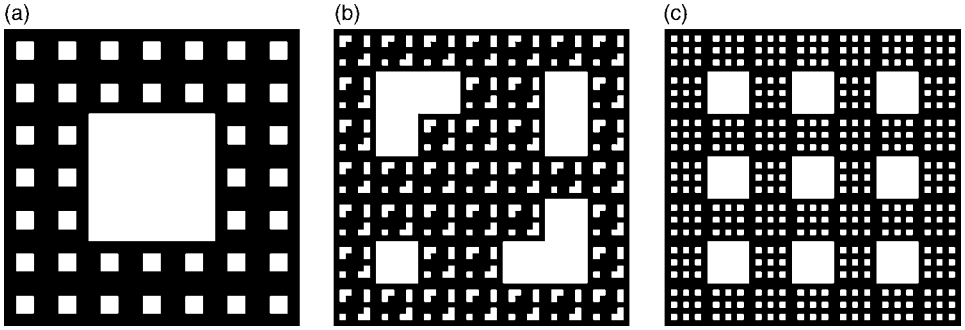

FIG. 1. Examples of second iterate prefractals of Sierpinski carpets having different appearances, but identical fractal (similarity) dimension. In all three cases, the iterative construction process consists of dividing the initiator in $7 \times 7 = 49$ squares, and removing $3 \times 3 = 9$ squares. This process is associated with a similarity dimension $D_s = \ln(49-9)/\ln(7) = 1.8957$.

deviation of a geometric object from translational invariance. In a low lacunarity object, where gap sizes are relatively homogeneous, different regions of the object tend to be similar to each other [as in Fig. 1(c)]. In contrast, in a high lacunarity object [like that in Fig. 1(a)], different regions may be very dissimilar and cannot be made to coincide by simple translation. This characterization of the translational invariance of geometric objects is highly scale dependent; objects that are heterogeneous at small scales, can be homogeneous when examined at larger scales or vice versa [16].

A method for calculating the lacunarity was outlined in general terms by Mandelbrot [13]. Subsequently, progress toward a usable method was made by Gefen *et al.* [16]. Allain and Cloitre [17] developed a straightforward algorithm, based on "gliding boxes" (or "moving windows") of increasing sizes, to evaluate the lacunarity of both deterministic and random fractals. More recently, Chappard *et al.* [18] described a different method to calculate the lacunarity, based on the mass-radius or sandbox algorithm used routinely to estimate fractal dimensions. Both of these algorithms have been used extensively in the literature, e.g., [19,20]. Yet fundamental questions remain unanswered concerning their robustness. In particular, it is unclear how much one should expect the lacunarities calculated by these algorithms to differ in specific cases. Perhaps more significantly, there is no information on the extent to which the lacunarity estimates yielded by current algorithms depend on the resolution of the images to which the algorithms are applied.

In this general context, the objective of the present paper is to analyze the effect of image resolution and of the choice of a particular calculation algorithm on estimates of the lacunarity of a number of porous media. The first section of this article, immediately following this introduction, describes succinctly the gliding-box algorithm as well as two variants of the sandbox algorithm. It also introduces two versions of a different algorithm that combines the geometry of the sandbox method with the statistics used in the gliding-box algorithm. Conversely, another algorithm is proposed that combines the geometry of the gliding-box method with the statistics used in Chappard *et al.*'s [18] algorithm. The next section describes the textbook Sierpinski carpet, the scanning electron micrograph of a soil thin section, and the light transmission photograph of a Togolese soil thin section, whose lacunarities are subsequently evaluated. The calculation results are analyzed critically in the last section, particularly in regard to the robustness of lacunarity estimates and to the possible usefulness of this parameter in future studies of the physical properties of porous media.

II. THEORY

A. The gliding-box algorithm

In this calculation method, suggested by Allain and Cloitre [17] and referred to in the following by the acronym (GLBA) a square structuring element or moving window of side length l is placed in the upper left-hand corner of an image of a solid geometrical structure of side length T (such that $l \leqslant T$). The calculation algorithm records the number or "mass" m of pixels that are associated with the solid underneath the moving window. The window is then translated by one pixel to the right and the underlying mass is again recorded. When the moving window reaches the right side of the image, it is moved back to its starting point at the left side of the image and is translated by one pixel downward. The calculation proceeds in this fashion until eventually the moving window reaches the lower right-hand corner of the image, at which point it has explored every one of its $(T-l+1)^2$ possible positions above the solid.

At that juncture, one may easily compute the number $n(m,l)$ of times a particular value of the mass m has been recorded with the moving window of side length l. Division of $n(m,l)$ by the total number $(T-l+1)^2$ of possible positions of the moving window above the image yields the probability distribution function $Q(m,l) = n(m,l)/(T-l+1)^2$. The statistical moments $Z_Q^{(q)}(l)$ of this probability distribution function are defined as

$$Z_Q^{(q)}(l) = \sum_m m^q Q(m,l) \tag{1}$$

where q equals 1 and 2 for the first and second moments, respectively, and the summation extends over all possible values of m (i.e., from 0 to l^2 for a moving window of side length l).

On the basis of these moments, Allain and Cloitre [17] define the lacunarity $\Lambda_{GB}(l)$, measured with a moving window of side length l, as

$$\Lambda_{GB}(l) = \frac{Z_Q^{(2)}(l)}{[Z_Q^{(1)}(l)]^2}. \tag{2}$$

Since the first moment $Z_Q^{(1)}$ is equal to the mean μ_Q of the probability distribution function Q, and the second moment $Z_Q^{(2)}$ is equal to the sum of the variance σ_Q^2 of Q and the square of the mean, i.e., $Z_Q^{(2)} = \sigma^2 + \mu^2$, one may rewrite Eq. (2) as

$$\Lambda_{GB}(l) = \frac{\sigma^2}{\mu^2} + 1 \tag{3}$$

which shows, perhaps more clearly than Eq. (2), that $\Lambda_{GB}(l)$ is fundamentally a relative measure of the width of the distribution $Q(m,l)$. For a translationally invariant set, it is straightforward to show that $Z_Q^{(2)}(l) = [Z_Q^{(1)}(l)]^2$. Under these conditions, $\Lambda(l)$ becomes identically equal to unity, and is independent of l [17].

B. Chappard *et al.*'s sandbox algorithm

The algorithm developed by Chappard *et al.* [18] is based on the sandbox method elaborated earlier by Tél *et al.* [21]. In the Chappard *et al.* sandbox algorithm (CSBA), a number s of points or "seeds" are selected randomly within the geometrical domain occupied by the object under study, with s taken either arbitrarily or equal to the number of seeds at which convergence is reached for a number of targeted summary statistics. Around each seed, k concentric circles are drawn and the mass m of the object that is contained in each circle is recorded as a function of the circle diameter l. Once this process has been carried out for all s seeds, one may compute a mass distribution $n(m,l)$ that depends on the mass m and circle diameter l. This mass distribution can readily be transformed into a probability distribution function $Q(m,l)$ via division by the number s of seeds, i.e., according to $Q(m,l) = n(m,l)/s$.

Using once again Eq. (1) to define the moments of the probability distribution function $Q(m,l)$ and remembering that the variance of $Q(m,l)$ is equal to the difference of $Z_Q^{(q)}(l)$ and $[Z_Q^{(q)}(l)]^2$, one finds easily that the coefficient of variation $\mathrm{cv}(l)$ of $Q(m,l)$ is given by

$$\mathrm{cv}(l) = \frac{\sigma}{\mu} = \frac{\sqrt{Z_Q^{(2)}(l) - [Z_Q^{(1)}(l)]^2}}{Z_Q^{(1)}(l)}. \tag{4}$$

This coefficient of variation is related to $\Lambda_{GB}(l)$ by the relation $\mathrm{cv}(l) = \sqrt{\Lambda_{GB}(l) - 1}$.

Chappard *et al.* [18] use this coefficient of variation to define their lacunarity L_C as follows:

$$L_C = \frac{1}{k} \sum_l \mathrm{cv}(l) \tag{5}$$

where the summation extends over all k circle diameters considered around the seeds.

At this point, two different versions of Chappard *et al.*'s sandbox algorithm can in principle be envisaged. The first version, denoted by CSBAo, constrains the seeds in such a way that they are located only on the geometrical object under study, and not in the gaps within the object. This restriction is commonly adopted in the literature, albeit never justified theoretically. The second version, labeled CSBAog, assumes on the contrary that seeds can be selected indifferently on the object or in the gaps. Comparison of Eqs. (2) and (5) makes it readily apparent that $\Lambda_{GB}(l)$ and L_C are fundamentally different concepts. Indeed, whereas $\Lambda_{GB}(l)$ depends on the side length l of the moving windows or structuring element, Chappard *et al.*'s lacunarity L_C does not depend on l, as a result of the averaging of $\mathrm{cv}(l)$ over the number of circle radii, k, in Eq. (5).

C. The modified sandbox algorithm

Since in the course of implementing the CSBA, one calculates a probability distribution function $Q(m,r)$ that is conceptually similar to that involved in the GLBA, it is in principle possible to apply to this second probability distribution the same statistical method [specifically, Eqs. (1) and (2)] that was used for the first. In other words, the first and second moments of the $Q(m,l)$ resulting from the sandbox algorithm can be computed according to Eq. (1) and introduced into Eq. (2) to yield a lacunarity $\Lambda_{SB}(l)$ that is dependent on l. As with the CSBA, the modified sandbox algorithm MSBA can be implemented using seeds belonging to both object and gaps, or using seeds belonging only to object. The algorithms associated with these two options will be referred to as MSBAog and MSBAo, respectively.

D. The modified gliding-box algorithm

The arguments presented in the preceding subsection to justify an additional algorithm for the calculation of the lacunarity can be applied symmetrically to the GLBA. The resulting algorithm is referred to as MGLBA. Instead of introducing the numerical values of the first and second moments of $Q(m,l)$ into Eq. (2) to compute $\Lambda_{GB}(l)$, one may introduce them in Eq. (4) to calculate a coefficient of variation $\mathrm{cv}(l)$. This coefficient of variation in turn may be used in an expression equivalent to Eq. (5) to define a lacunarity parameter L_{GB}, which can be directly compared to Chappard *et al.*'s [18] L_{SB}.

III. IMAGES AND LACUNARITY CALCULATIONS

A. Images of the Sierpinski carpet prefractal

The first set of images analyzed in the present article is related to the traditional Sierpinski "carpet" (Fig. 2), a textbook geometrical fractal described in detail in many publications, e.g., [4,13]. The iterative procedure that leads to this carpet starts with a square initiator of side length L. In the first step in the iteration (called the generator), this square is partitioned into nine subsquares of side $L/3$ and the center subsquare is removed. In the subsequent step, the generator is applied to each remaining square of side $L/3$, i.e., it is again partitioned into nine subsquares of side $L/3^2 = L/9$, and the center subsquare is removed. When one applies this same iterative process *ad infinitum* to the remaining squares, the Sierpinski carpet is obtained. It has a similarity dimension equal to $\ln(8)/\ln(3) = 1.89$, a vanishing area, and a porosity (area of openings or voids divided by the total area of the square initiator) equal to 1, whereas the total perimeter of its holes is infinite.

Since the real Sierpinski carpet cannot be represented graphically, an image of its highest iterate, the eighth, that is manageable computationally with a desktop computer, was considered in the analysis. It has 6561×6561 pixels. Four

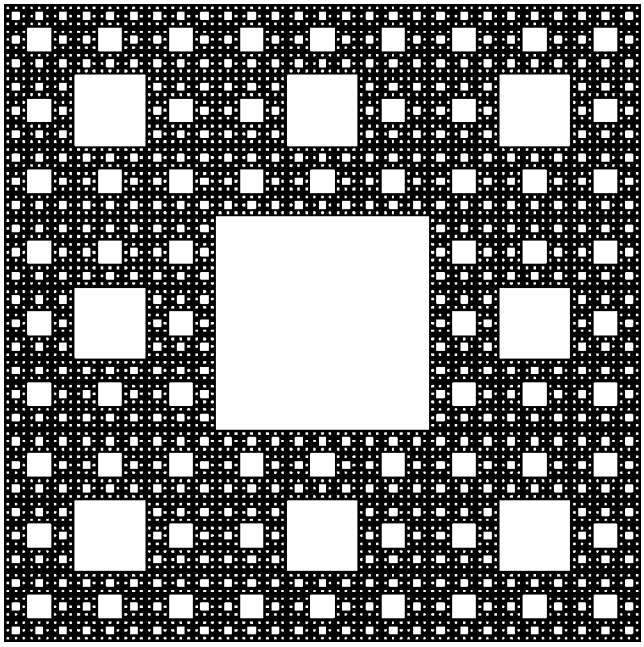

FIG. 2. Illustration of the fifth iterate prefractal of the classical Sierpinski carpet, with 243×243 pixels. Black pixels represent the carpet, whereas white pixels are associated with gaps or voids.

"snapshots" of this image were taken. Two of the snapshots were of size 6144×6144 pixels (which is divisible by multiples of 2), and two were of size 5120×5120 pixels. Of these snapshots, two, denoted 6144_1 and 5120_1, were concentric with the original image, whereas the other two, denoted 6144_2 and 5120_2, were centered about a randomly selected point. Since results were similar with all four snapshots, only one of them (6144_1) is considered in the following. The resolution of this snapshot was coarsened by factors of 2, 4, and 8 (see Table I for details). Coarsening refers to resampling of the original image in order to produce a new image of lower resolution. This procedure was carried out with the bilinear algorithm, implemented, e.g., in the image manipulation software Adobe PHOTOSHOP. After coarsening, images need to be thresholded to obtain binary images. This thresholding was performed separately for every image. Thresholding to obtain binary images was done separately for every image by using an arbitrary gray value of 128 (middle of the full spectrum) as the threshold. Application of a less arbitrary thresholding method (described below) confirmed that the midpoint gray value was acceptable to threshold the images. In the resulting binary images, a pixel value of 1 is associated with the Sierpinski carpet prefractal, and a value of 0 corresponds to a hole or gap.

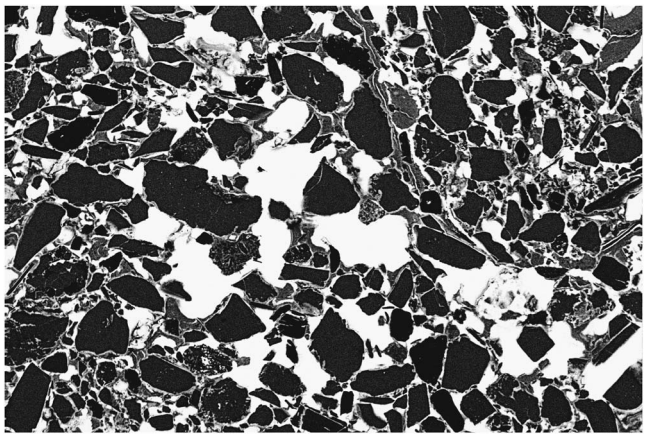

FIG. 3. Thresholded scanning electron micrograph of a thin section of Central European soil. The soil particles are black and the pores or voids are white.

B. Scanning electron microscope images of soil thin section

An original scanning electron microscope (SEM) image (Fig. 3) was obtained from a thin section of a block of soil impregnated with resin. The soil block originated from the Bt horizon of a Luvisol, developed on Loess, sampled in Central Europe in the county of Göttingen, Germany. This specific soil horizon contains approximately 20% clay, 70% silt, and 10% sand according to the German soil taxonomy. The image, showing the surface of the soil thin section with a depth of focus of about 1 μm, was taken with a field emission scanning electron microscope (FESEM), and resulted from a combination of 75% backscattered and 25% secondary electrons. The image corresponds to a 544×363 μm^2

TABLE I. Image sizes (in pixels) for the snapshots of the Sierpinski carpet, the SEM images of the soil thin section, and the light transmission photographs (LTPs) of the Togolese soil.

Coarsening factor	Sierpinski carpet	SEM (European soil)	LTP (Togolese soil)
1	6144×6144	3072×5072	8000×5060
1.5		2048×1368	
2	3072×3072		4000×2530
3		1024×684	
4	1536×1536		2000×1265
5			1600×1012
6		512×342	
6.67			1200×759
8	768×768		
10			800×506

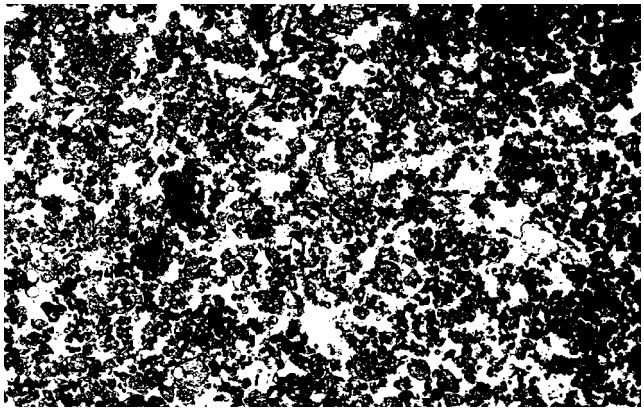

FIG. 4. Thresholded light transmission photograph of a thin section of Togolese soil. The soil particles and aggregates are black, and the pores or voids are white.

portion of the thin section and contains 3072×2052 pixels. It was coarsened by factors of 1.5, 3, and 6 [8].

To threshold or "segment" a digitized image, one could in principle proceed by trial and error until one achieves a thresholding that appears reasonable, i.e., coincides with some *a priori* idea one may have about the two categories of pixels one attempts to separate. Unfortunately, this procedure is very subjective and may lead to biases when one is trying to compare images, or in the analysis of time sequences of images of a given object, e.g., under evolving lighting conditions. To palliate these difficulties, numerous automatic, nonsubjective thresholding algorithms have been developed, e.g., [22]. One of the most commonly used algorithms, referred to as the "minimum error algorithm," is adopted in the research described in the present article. According to this algorithm, the histogram associated with an image is visualized as consisting of two usually overlapping Gaussian distributions. A starting guess for the threshold is made. The fraction of the pixels in each of the two sets of pixels defined by this threshold is calculated, as are the mean and variance of each of the sets. Then, in effect, a composite histogram is formulated, which is a weighted sum of two Gaussian distributions, each with mean and variance as just calculated, and weighted by the calculated fraction. The gray-scale level at which these two Gaussian distributions are equal is estimated via solution of a quadratic equation. This gray-scale level, truncated to an integer, gives the next guess for the threshold. Again, the process is continued, iteratively, until it converges. In its original formulation, the minimum error algorithm suffers from the fact that the choice of the starting guess used to initiate the iterative calculations influences the convergence to a final threshold value. The resulting indeterminacy was avoided by using an objective approach developed by Boast and Baveye [23].

C. Transmitted light photograph of a thin section of a Togolese soil

The light transmission photograph of the Togolese soil (Fig. 4) was obtained by placing directly on a piece of photographic paper and illuminating for a set time a resin-impregnated thin section of a sample of soil obtained in 1992 in the research station of the Institut National des Sols at Glidji (Aneho), in the "terres de Barre" region of southern Togo (see [24] for further details). A portion of the photograph representing a 24.6×14.6 mm^2 area of the thin section was scanned at different resolutions with a digital scanner, to produce a set of images with dimensions of 8000×5060, 4000×2530, 2000×1265, 1600×1012, 1200×759, and 800×506 pixels, respectively. These images were thresholded with the minimum error algorithm described in the previous section, to produce binary images suitable for lacunarity evaluation.

D. Lacunarity calculations

Measurements with the gliding-box algorithms were carried out with a minimum of 11×11 to 31×31 pixels, depending on image size, and a maximum box size of 301×301 pixels. Both limits were adjusted to keep computation time manageable. The sandbox algorithms were implemented using a minimum circle diameter of at least 11 pixels, and a maximum circle diameter of approximately one-fifth the largest dimension of the image. Again both limits were adjusted to keep computation time manageable. Circle diameters were incremented by multiples of ten pixel sizes around each seed, until they reached the edges of the image. This typically resulted in between 10 and 30 concentric circles around each seed, depending on image size. This procedure was repeated for 50 to 700 seeds in increments of 50 seeds, i.e., 14 distinct measurements, which were subsequently averaged.

IV. RESULTS AND DISCUSSION

In order to compare the lacunarity of images having different pixel sizes, we systematically multiplied the size of the moving window by the image coarsening factor. For instance, a gliding-box size of 101×101 pixels for an image that was coarsened by a factor of eight is equivalent to a gliding-box of size $8(101 \times 101) = 808 \times 808$ pixels for the image before it was coarsened. This referencing of the side length of the gliding boxes, and of the diameter of sand boxes, to numbers of pixels in the original image affords a convenient basis for the comparison of different algorithms, particularly their visual comparison as in Figs. 5–8.

Calculation results obtained in the case of images of the Sierpinski carpet (Fig. 5) show that the lacunarities measured with the gliding-box algorithm decrease monotonically when the side length of the gliding boxes is increased. At any given side length, the lacunarity increases significantly as the resolution is decreased. For example, at a normalized side length of 100 pixels (in the original image), the lacunarity for the 768×768 image is 11.6% larger than that for the higher-resolution 6144×6144 image. The lacunarity of the high-resolution Sierpinski carpet images decrease at a slower rate than it does for low-resolution Sierpinski carpet images. If one extrapolates to higher side lengths the data for the highest resolutions, the lacunarities of all the images appear to converge near a normalized gliding-box side length of 2511 $[(\log_{10}(2511) \approx 3.34]$.

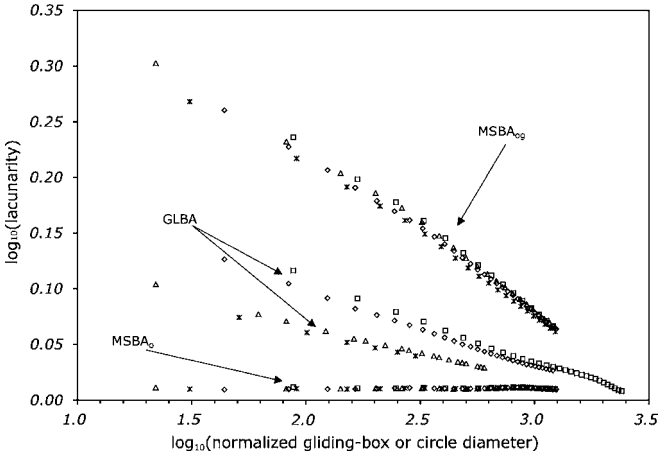

FIG. 5. Lacunarity measured by the gliding-box algorithm (GLBA) and by the modified sandbox algorithm (MSBA), both with seeds only on the object (MSBAo) and on the object and in the gaps (MSBAog), of the Sierpinski carpet images 6144×6144 (*), 3072×6072 (△), 1536×1536 (◇), and 768×768 (□).

The lacunarities of the Sierpinski carpet images evaluated with the modified sandbox algorithm with seeds both on the object and in the gaps (MSBAog) also decrease systematically as the diameter of the sandboxes is increased. However, in this case, the decrease is much more pronounced, from lacunarity values close to 2.0 $[\log_{10}(2.0)\approx0.30]$ for small sandboxes, to values near 1.12 $[\log_{10}(1.12)\approx0.05]$ at the other end of the range of sandbox diameters considered. At a normalized sandbox diameter of 100 pixels (in the original image), the lacunarity associated with the 768×768 image is merely 4.2% larger than that for the higher-resolution 6144×6144 image, and that difference decreases with increasing sandbox diameter.

Measurements of the lacunarity of images of the Sierpinski carpet with the MSBAo algorithm differ appreciably, both qualitatively and quantitatively, from those obtained

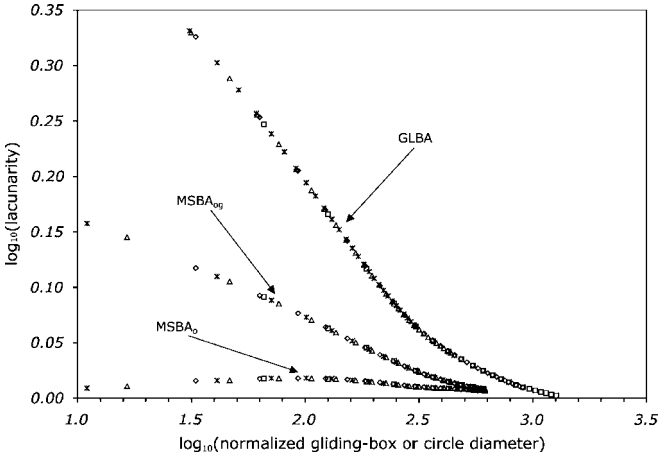

FIG. 6. Lacunarity measured by the gliding-box algorithm (GLBA) and by the modified sandbox algorithm (MSBA), both with seeds only on the object (MSBAo) and on the object and in the gaps (MSBAog), of the SEM images 3072×2052 (*), 2048×1368 (△), 1024×684 (◇), and 512×342 (□).

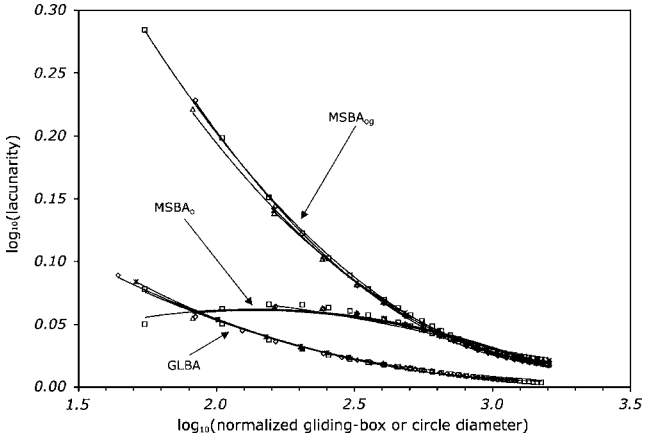

FIG. 7. Lacunarity measured by the gliding-box algorithm (GLBA) and by the modified sandbox algorithm (MSBA), both with seeds only on the object (MSBAo) and on the object and in the gaps (MSBAog), of the light transmission photographs of the Togolese soil with dimensions 8000×5060 (*), 4000×2530 (△), 2000×1265 (◇), and 1600×1012 (□).

with the GLBA or MSBAog. Lacunarities are restricted to a narrow domain (between 1.022 and 1.027), near the lowest values obtained by GLBA, and very close to the minimum value possible for $\Lambda(r)$ of 1. That lacunarities evaluated with MSBAo are systematically lower than those calculated with MSBAog can be explained by the fact that selection of seeds belonging only to the object greatly increases the mass in each sandbox, and therefore increases $Z_Q^{(1)}(l)$, which in turn lowers the ratio of Eq. (2), driving downward the value of lacunarity. In the narrow range spanned by the MSBAo lacunarity in Fig. 5, lacunarities do not increase or decrease monotonically. Close inspection reveals that three local maxima occur in the vicinity of sandbox diameters of 100, 250, and 790 pixels $[(\log_{10}(l)=2.0,\ 2.4,$ and 2.9, respectively]. These maxima may be related to the largest gap sizes in the Sierpinski carpet, which are 81×81, 243×243, and

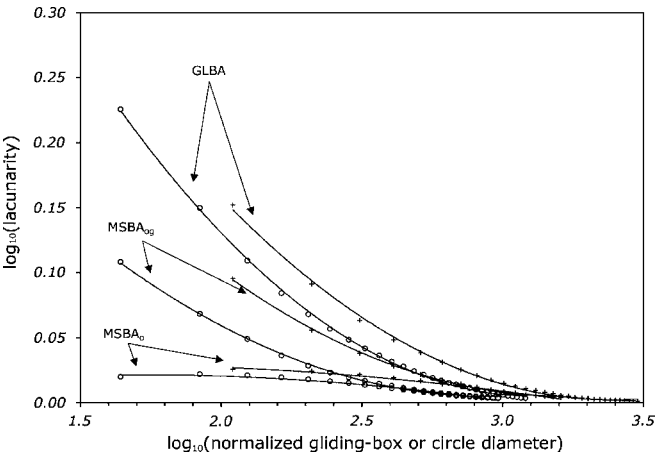

FIG. 8. Lacunarity measured by the gliding-box algorithm (GLBA) and by the modified sandbox algorithm (MSBA), both with seeds only on the object (MSBAo) and on the object and in the gaps (MSBAog), of the light transmission photographs of the Togolese soil with dimensions 1200×759 (○) and 800×506 (+).

729×729 pixels. By comparison with results obtained with the GLBA and MSBAog algorithms, lacunarities of the Sierpinski carpet images evaluated with the MSBAo algorithm do not discernibly depend on image resolution.

One possible explanation of the strong effect of resolution on the lacunarity estimated with the GLBA algorithm, and of the absence of a similar effect on the estimates produced by the MSBAog and MSBAo algorithms, is related to the shape of the structuring elements used. A square structuring element used to measure an image made up of squares may magnify distortions caused by coarsening. Coarsening of images involves the combination of pixels and the arithmetic averaging of their gray values. This process, along with the subsequent thresholding needed to produce a binary image, progressively distorts the small-scale structure of the object represented in the image. For example, square structures or gaps initially present in an image may be transformed into "L" or "+" shapes after coarsening. As this happens, the mass of the object contained in a gliding box or sandbox may be affected significantly, and this effect may depend on the shape of the structuring element. The hypothesis that the shape of the structuring element affects the degree to which the resolution of an image influences lacunarity measurement is supported empirically by the measurements of Sierpinski carpets by MSBAog (Fig. 5). For a normalized structuring element size of $l=100$, these measurements show an average difference in lacunarity of less than 2% between images at different resolutions, whereas GLBA results differ by as much as 11%. MSBAog uses the same statistics as GLBA [Eq. (2)], but samples the object with circular structuring elements instead of square ones. The sampling in MSBAog is carried out randomly, but this appears not to be of much consequence, since measurements by this algorithm were made for several numbers of seeds (50–700) and did not lead to great differences in values among measurements of the same image.

Unlike in the case of the Sierpinski carpet images, the lacunarities associated with the SEM images of the Central European soil (Fig. 6) do not appear affected to any significant extent by the resolution of the images. Also unlike in the previous case, the lacunarities evaluated with the GLBA algorithm are markedly larger than those measured with the MSBAog algorithm. The latter lacunarities are, however, once again significantly larger than the values obtained with the MSBAo algorithm, to which they eventually converge as the sandbox diameters increase. This convergence is not surprising since it is reasonable that as the diameter of sandboxes increases, the exact location of the center of the sandboxes, whether on the object or in the gaps, becomes less and less significant. The lacunarities evaluated with the MSBAo algorithm are, in this case also, confined to a narrow range (between 1.015 and 1.042), in which they exhibit a concave curve, with a single maximum at a normalized sandbox diameter close to 60 pixels $[\log_{10}(60)\approx 1.78]$, corresponding to 10 μm.

Application of the minimum error thresholding algorithm to the images obtained by scanning the light transmission photograph of the thin section of the Togolese soils resulted in very different thresholds for the images of size 800×506 and 1200×759 pixels compared to the other images. In the two low-resolution images, the optimal threshold calculated by the minimum error algorithm corresponded to gray-scale values of 224 and 228, respectively, for the 800×506 pixel and for the 1200×759 pixel images, whereas it was equal to 188 for the 1600×1012 pixel image, and to 189 for the higher-resolution images. Slight differences between the histograms of the various images probably account for the discrepancy among the thresholds.

These differences in threshold values lead to significant differences in the behavior of the lacunarity algorithms, as shown in Figs. 7 and 8. In the four highest-resolution images (Fig. 7), contrary to what was observed with the Sierpinski carpet (Fig. 5) and particularly with the SEM images (Fig. 6), the GLBA algorithm yields the lowest lacunarity values in most of the range of gliding box sizes considered, compared to the MSBAog and MSBAo. The MSBAo algorithm yields lacunarity curves that are markedly concave, unlike the other two algorithms, which produce convex curves, pointing upward at small sandbox diameters or gliding-box side lengths. As in Figs. 5 and 6, the curves obtained by the MSBAog and MSBAo algorithms converge at the upper end of the range of sandbox diameters. Furthermore, all three algorithms yield lacunarity estimates that seem independent of image resolution. The slight differences in the lacunarity of the various images evaluated by the MSBAog at low sandbox diameters are somewhat erratic and do not follow a particular trend with image resolution.

In a number of respects, both qualitatively and quantitatively, the situation is very different for the two low-resolution images (Fig. 8). The lacunarities estimated by the GLBA algorithm are now consistently the highest, and the lacunarities evaluated with the MSBAog and MSBAo algorithms are significantly lower than those displayed in Fig. 7 over the whole range of sandbox diameters considered. In the two low-resolution images, all three algorithms also appear affected by image resolution, with the lacunarities of the coarser-resolution image (800×506) being systematically higher than that of the 1200×759 image. These observations may reflect a direct dependence of lacunarity on resolution, which becomes noticeable in coarse-resolution images, or it may be the quantitative expression of the opening up of pores that resulted from the higher threshold in the 1200×759 pixels image.

Up to this point, the discussion about the effect of image resolution on lacunarity estimates has been confined to marked differences in the positions of the different lacunarity curves. There is, however, a more subtle effect of resolution on the lacunarity estimates computed by the GLBA, the MSBAog, and the MSBAo algorithm, which needs to be acknowledged as well. In all three cases, for practical reasons, it is reasonable to constrain the upper end of the range of gliding-box side lengths or sandbox diameters that is used in the calculations to be smaller than an arbitrary fraction of the size of the original, uncoarsened image. Under these conditions, this upper size of the gliding boxes or sandboxes is independent of image resolution. However, a clear rationale is lacking to also impose that the lower end of the range be the same for all images. Theoretically, this lower limit could go down to the size of individual pixels in each image, which means that it could vary by as much as a factor of ten (or one

$\log_{10}$ unit) in Figs. 5–8. In some cases, this can lead to lacunarity values varying by 33% at the lower limit, given the convex shape of the curves.

In terms of the overall ranking of the three sets of images on the basis of their lacunarity, cross comparison of Figs. 5–8 shows that for the GLBA, this ranking depends on the range of gliding-box side lengths that one considers. In the low range (small side lengths), the SEM images have by far the highest lacunarity, followed by the Sierpinski carpet images and by the higher-resolution Togo images. In the high range of gliding-box side lengths, the SEM images drop to the bottom of the pack. The low-resolution Togo images exhibit a behavior that is intermediate between the SEM images and the Sierpinski carpet at small gliding-box side lengths, and lies between the other two sets of curves at large gliding-box side lengths. Calculations with the MSBAog suggest that the Sierpinski carpet images have the highest lacunarity throughout the range of sandbox diameters considered, followed relatively consistently by the higher-resolution Togo images, the SEM images and the lower-resolution Togo images. Given the narrowness of the range of lacunarities produced by the MSBAo, rankings of the three sets of images may be less meaningful in this case. Nevertheless, the higher-resolution Togo images appear to have a slightly higher lacunarity than the other curves over the whole range of sandbox diameters considered, followed by the lower-resolution Togo images, the SEM images, and the Sierpinski carpet images. These ranking results suggest that there is no simple answer to the question of which one of the three systems depicted in Figs. 2–4 is the most "lacunar." Each algorithm tested provides a slightly different answer.

The strong scale dependence of the lacunarity, as calculated by the GLBA, the MSBAog, and MSBAo, raises the question of the usefulness of this index to characterize natural systems. The initial concept of lacunarity, sketched by Mandelbrot [13], was that of a single number that, in combination with a fractal dimension, could completely encapsulate the geometry of any given system and serve to predict some of its other characteristics (e.g., transport or dielectric properties in porous media). It is unclear how a strongly scale-dependent lacunarity would be used for the same purpose. If one does not try to reduce it to a single number (as is done in the CSBA and MGLBA, or alternatively by approximating the lacunarity curves by straight lines and by using the slope of these lines as an indicator of translation invariance), there may not be any significant advantage in calculating lacunarities, compared with looking at the systems under study through the lens of multifractal measures, e.g., [4,10]. Further research is needed to determine which approach is the most useful in practice to describe porous media.

The results obtained with the last two algorithms, the CSBA and the MGLBA (Fig. 9), cannot be directly compared with those of the other algorithms, since both the CSBA and the MGLBA provide single lacunarity estimates, independent of either the diameter of sandboxes or the side length of gliding boxes. When the resolution decreases (i.e., when the coarsening factor increases in Fig. 9), the lacunarity calculated with the CSBA remains virtually constant in a

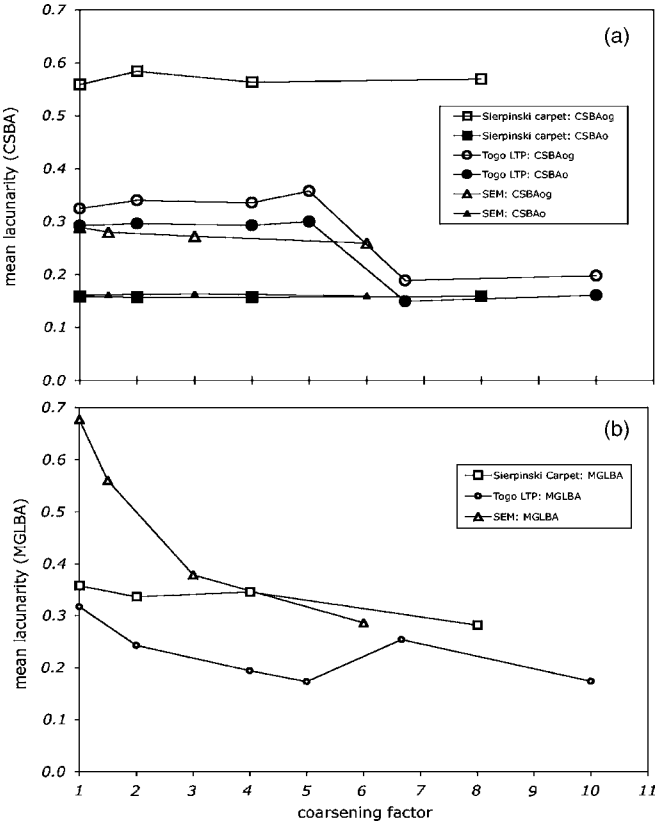

FIG. 9. (a) Mean lacunarity measured by the Chappard sandbox algorithm (CSBAo and CSBAog) for images at different resolutions (coarsening factors). Solid symbols represent images measured with CSBAo and hollow symbols represent objects measured with CSBAog. (b) Lacunarity measured with the modified gliding box algorithm (MGLBA).

number of cases. For the SEM images, when seeds are taken both in the object and in the gaps, calculation results indicate that the lacunarity decreases slightly with decreasing resolution. The only case where a decrease with resolution is marked is for the Togo images, regardless of how the seeds are selected. The lacunarity for the two coarser-resolution images are significantly lower than for the other images of the same thin section.

Aside from this effect of resolution, the Sierpinski carpet has by far the largest lacunarity when seeds are taken both in the object and in the gaps (open squares in Fig. 9), and the SEM and the Togo images have commensurate, lower lacunarity in that case. By contrast, when seeds are selected only in the object, the higher-resolution images of the Togo soil have the highest lacunarity, and the Sierpinski carpet and the SEM images have virtually identical, much lower lacunarity. At the highest coarsening factors, CSBAo does not appear able to discriminate between the three natural porous media; their lacunarity appears identical.

For the lacunarity calculated with the MGLBA, a decrease with decreasing image resolution appears to be the rule rather than the exception (Fig. 9, bottom graph). The decrease is particularly marked (from 0.675 to 0.26) for the SEM images. For the Togo images, passage from the 1600 $\times$ 1012 pixel image (coarsening factor 5) to the 1200

$\times 759$ pixel image (coarsening factor 7) results in an increase of the lacunarity, unlike in the case of the lacunarity values obtained with the CSBA (Fig. 9, top graph). Because of these different trends, the rankings of the lacunarities of the Sierpinski carpet, the SEM images, and the Togo pictures change with image resolution. At the high-resolution end (low coarsening factor), the SEM images are the most lacunar, followed by the Sierpinski carpets and the Togo images. At the lower resolutions, the lacunarity of the SEM images drops below that of the Sierpinski carpets, at least, and seems destined to get lower than that of the Togo pictures as well.

The results obtained with the CSBA and the MGLBA suggest that researchers interested in characterizing the properties of porous media and who would like to know if a single, scale-independent lacunarity measure could be useful for their purposes, should probably adopt the CSBAog, which appears to provide consistent, differentiated information. Like the other algorithms analyzed here, this algorithm suffers from the fact that gray-scale images need to be thresholded before they can be analyzed, giving rise occasionally to artifactual variations of the resulting lacunarity, as in the case of the Togo images. This operational shortcoming might be resolved by adoption of one of the many sophisticated image segmentation algorithms that have been developed in recent years, e.g., [22,25].

V. CONCLUSIONS

In the present paper, six different calculation algorithms are applied to binary images of three different systems (a theoretical fractal and two natural porous media). The calculation results suggest that lacunarity estimates, as well as the determination of the ranking of the three tested systems according to their lacunarity, are affected strongly by the algorithm used, by the resolution of the images to which these algorithms are applied, and, at least for three of the algorithms (producing scale-dependent lacunarity estimates), by the scale at which the images are observed. Depending on the conditions under which the estimation of the lacunarity is carried out, lacunarity values range from 1.02 to 2.14 for the three systems tested, and all three of the systems can be viewed alternatively as the most or the least "lacunar." Among the algorithms that produce a scale-invariant lacunarity, the Chappard sandbox algorithm (CSBAog), with seeds selected both in the object under study and in the gaps, appears to be the most reliable option. Further research will be needed to determine if the estimation of scale-dependent lacunarities, for example with algorithms GLBA, MSBAog, or MSBAo, presents practical advantages over the calculation of the multifractal $f(\alpha)$ spectrum [26,27] in the case of porous media.

ACKNOWLEDGMENTS

We are grateful to the National Science Foundation for partial support of D.E.P. under Grant No. DGE-9870631 (IGERT Program in Nonlinear Systems), and to the German Science Foundation (DFG) for partial support of A.D. under Grant No. DA 575/1-1. Sincere gratitude is also expressed to Professor Hudson Kern Reeve, Dr. Martin Thullner, and Robyn Miller for many helpful suggestions and stimulating discussions.

[1] J. Giles, Nature (London) **432**, 267 (2004).
[2] D. H. Rouvray, Endeavour **20**, 79 (1996).
[3] O. R. Shenker, Stud. Hist. Philos. Sci **25**, 967 (1994).
[4] P. Baveye and C. W. Boast, in *Fractals in Soil Science*, edited by P. Baveye, J.-Y. Parlange, and B. A. Stewart (CRC Press, Boca Raton, FL, 1998), pp. 1–54.
[5] S. Ogawa *et al.*, Geoderma **88**, 109 (1999).
[6] B. H. Kaye, *A Random Walk through Fractal Dimensions* (VCH Verlagsgesellschaft, Weinheim, Germany, 1989).
[7] P. Baveye *et al.*, Water Resour. Res. **34**, 2783 (1998).
[8] A. Dathe and P. Baveye, Eur. J. Soil. Sci. **54**, 453 (2003).
[9] J. Fridrich, Int. J. Gen. Syst. **25**, 245 (1996).
[10] H. Grout, A. M. Tarquis, and M. R. Wiesner, Environ. Sci. Technol. **32**, 1176 (1998).
[11] Q. Huang *et al.*, Pattern Recogn. **27**, 339 (1994).
[12] H. F. Jelinek and E. Fernandez, J. Neurosci. Methods **81**, 9 (1998).
[13] B. Mandelbrot, *The Fractal Geometry of Nature* (W. H. Freeman and Co., New York, 1982).
[14] B. Mandelbrot and D. Stauffer, J. Phys. A **27**, L237 (1994).
[15] B. B. Mandelbrot, A. Vespignani, and H. Kaufman, Europhys. Lett. **32**, 199 (1995).
[16] Y. Gefen, Y. Meir, B. B. Mandelbrot, and A. Aharony, Phys. Rev. Lett. **50**, 145 (1983).
[17] C. Allain and M. Cloitre, Phys. Rev. A **44**, 3552 (1991).
[18] D. Chappard *et al.*, J. Pathol. **195**, 515 (2001).
[19] R. E. Plotnick, R. H. Gardner, and R. V. Oneill, Landscape Ecol. **8**, 201 (1993).
[20] R. E. Plotnick, R. H. Gardner, W. W. Hargrove, K. Predegard, and M. Perlmutter, Phys. Rev. E **53**, 5461 (1996).
[21] T. Tel, A. Fulop, and T. Vicsek, Physica A **159**, 155 (1989).
[22] P. Baveye, Water Res. **36**, 805 (2002).
[23] C. W. Boast and P. Baveye, Int. J. Pattern Recognit. Artif. Intell. (to be published).
[24] C. L. Bielders *et al.*, Soil Sci. Soc. Am. J. **60**, 843 (1996).
[25] X. Cufi, *et al.*, Adv. Imaging Electron Phys. **120**, 1 (2002).
[26] A. Saucier, Physica A **183**, 381 (1992).
[27] A. Saucier *et al.*, Physica A **311**, 231 (2002).